

Advanced Plasticity & Fracture for Structural Car Body Metals in Crashworthiness CAE analysis: SAMP-1 plus GISSMO

Alejandro Domínguez^a, Pablo Cruz^a, Lluís Martorell^a, Adrián Ros^a, Eduardo Martín-Santos^a

Courtesy of: Andrew Hall^b, Patrick Kelly^b, Ilyasuddin Syed^b

^aApplus IDIADA

^bFaraday Future

1 Introduction

This paper describes an engineering process to generate material cards for forefront crashworthiness CAE analysis that properly capture both plastic and fracture behaviour of car body structural metals. The main objective of the paper is to show that advanced plasticity approaches can be used without significantly increasing the complexity of the overall material characterization process. The paper is mainly centred in metals plastic characterization for shell elements although some important relationships with the fracture characterization will be also discussed. Before defining the engineering process, it is necessary to tackle some misleading general ideas that the automotive CAE community normally assumes as correct for metals like steel or aluminium alloys. The criticized assumptions read:

- Metals plasticity can be comprehensively defined with the stress-strain curves obtained from uniaxial tension tests
- Coupon tests make the specimen work under a “pure” and constant loading mode state of stress. The stress versus plastic strain obtained directly from the coupon test results can be used as input curves in the material cards

These assumptions limit both the understanding of the CAE engineers of the actual metals behaviour and the efficiency of the designs in terms of structural performance and weight. Additionally, these assumptions inject inaccuracies in the CAE solutions that are normally balanced in the fracture definition which can lead to more numerical difficulties and less reliable CAE results.

In automotive full vehicle crash CAE models, most of the body structural metal parts are represented using MAT 24. This fact has influenced the concentration of significant efforts in the numerical efficiency and stabilization of MAT 24 inside the CAE solvers. Therefore, the automotive CAE community uses MAT 24 when feasible because it provides a very efficient, robust and well-known tool. The generation of material cards has been and will always be one of the cores of a reliable CAE model. During the last decades the construction of the MAT 24 material card has become a standard in solver user's books with a clear and straightforward explanation regarding the generation of the stress versus plastic strain inputs starting from the uniaxial tension experimental data. Let us call this approach the “classic” experimental data post-process. The clarity and simplicity of the classic approach have created a fake sense of control of the correct definition of the plastic behaviour of the body structural metal parts. Additionally, it is generally accepted the assumption that the plastic behaviour of structural metals can be fully characterized only providing to the material law the stress versus plastic strain inputs from the uniaxial tension case.

Experimental results show that metals like aluminium alloys and steel alloys exhibit an independent yield behaviour for different loading modes. Thus, it is necessary to provide to the material law the stress versus plastic strain inputs of the relevant loading modes to obtain accurate crashworthiness CAE results. For these metals, the use of a material law that includes

a *Multi-Loading-mode-Yielding* plasticity model is certainly necessary. A *Multi-Loading-mode-Yielding* plasticity model can be calibrated with the same coupon test matrix as the one used for the calibration of the fracture models like Gissmo or DIEM. Therefore, in general there is no need of enlarging the coupon test matrix for a *Multi-Loading-mode-Yielding* plasticity calibration when fracture calibration is also required.

When looking for reliable LS-Dyna material laws that consider a *Multi-Loading-mode-Yielding* plasticity model, SAMP-1 is a clear candidate. Nevertheless, the user input flexibility of SAMP-1 material card may lead to inconsistent definitions and undesired numerical instabilities or lack of reliability. The main difficulties in the use of SAMP-1 are:

- The user can enter up to 4 independent stress-strain curves for different loading modes. Most of the literature about SAMP-1 seems to propose the direct use of the stress-strain curves obtained from the classic experimental data post-process of different coupon tests results. The application of this approach can be a source of inconsistencies, numerical issues, and lack of reliability of the material card. The principal reason for the generation of inconsistencies is the fact that the material card needs the definition of 4 stress-strain curves obtained from the material working under pure and constant loading modes and the coupon test setups are most of the times far from providing pure loading mode experimental data even when the tests are properly carried out.
- The user is not supported in the construction of the 4 stress-strain input curves to respect the mandatory interrelationships imposed by SAMP-1 hardening rule regarding the plastic strain evolution for different loading modes due to the strain hardening (i.e. yield stress surface growth). This fact provides unwanted freedom that allows the definition of inconsistent input data without warnings.
- The experimental measurement of the plastic Poisson's ratio is not clearly explained in the literature. The lack of clear definition together with the fact that deep understanding of the DIC tools is necessary to measure the plastic Poisson's ratio lead to additional numerical inconsistencies in the input data (please see [1]).

This paper proposes a user-oriented approach that may allow SAMP-1 to become the standard for car body metal structural parts in crashworthiness CAE analysis.

The overall approach described in this paper is validated for shell-based CAE models.

2 Coupon level experimental campaign

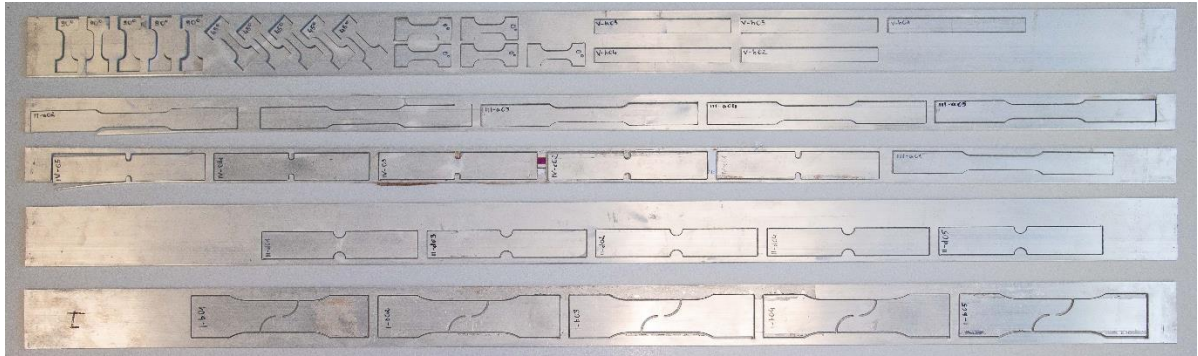
This paper is illustrated with an aluminium extrusion alloy characterization. The characterization approach described in the paper is also valid for steels or any other metal from the car body. The aluminium alloy shown in this paper does not present strain rate hardening. Therefore, the complete coupon test campaign is carried out in quasi-static conditions. The coupon level experimental campaign for both fracture and plastic characterization is described in the table below.

Quasi-static Coupon Tests
Smooth tensile ASTM E8
Tensile 0°, 45° & 90° ISO 8256 Type 3
Shear 0°
Small notch tensile
Large notch tensile
3-point bending ASTM D790



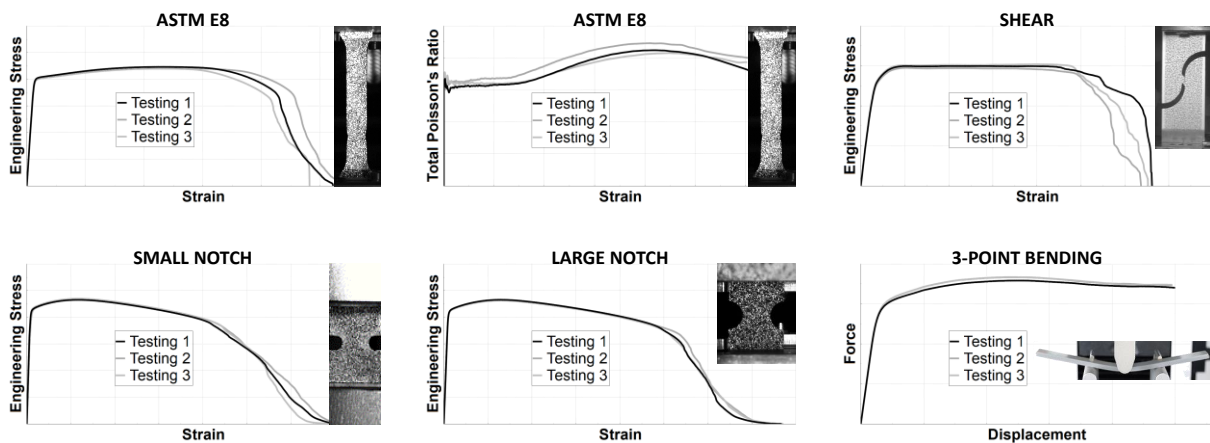
Coupon specimens. Courtesy of Faraday Future

All coupons are machined from the original extruded aluminium component (as shown in the figure below).



Coupon specimens extracted from the component. Courtesy of Faraday Future.

Coupon level experimental results are shown in the figures below. All coupon tests were carried out at Applus DatapointLabs.



Coupon test results. Courtesy of Faraday Future

From the engineering point of view, it is important to define a process that allows the CAE engineers the assessment of the coupon experimental results to understand how the material yielding depends on the loading modes and whether MAT 24 plasticity assumptions are acceptable, or it is necessary to use a material law that includes a *Multi-Loading-mode-Yielding* plasticity model. A proposal of this process is done in the following sections.

2.1 Multi-Loading mode plasticity assessment: the σ_{vm} - p diagram

The σ_{vm} - p diagram is an engineering tool that helps in the understanding of the material plastic behaviour regarding the yield stress of the material when working under different loading modes. Thus, it provides a graphic support to the decision of using either MAT 24 or SAMP-1. In short, for MAT 24 and SAMP-1, the σ_{vm} - p diagram describes the complete material yield stress surface in the principal stress space by means of representing the generatrix of the two yield stress revolution surfaces with respect to the hydrostatic axis (considering that $\|\sigma_H\|^* = \sqrt{3} p$ and $\|S\| = \sqrt{2/3} \sigma_{vm}$. Please refer to [3]).

This paper is only focused on the plasticity models of MAT 24 and SAMP-1 using the piecewise-linear yield surface option (i.e. nonzero RBCFAC and four user-input curves LCID-T, LCID-C, LCID-S, and LCID-B defined). For other plasticity models not considered in the scope of this paper the conclusions of this section may be incomplete.

For any given stress state σ , the mean stress σ_m (or the pressure $p = -\sigma_m$) can be always obtained as the average of the stress tensor trace (tensor magnitudes in compact notation denoted by bold font). The hydrostatic stress state is defined as the loading mode where the material works under the mean stress from all directions.

$$\sigma_m = -p = \frac{1}{3} \text{tr}[\sigma] \Rightarrow \sigma_H = \begin{bmatrix} \sigma_m & 0 & 0 \\ 0 & \sigma_m & 0 \\ 0 & 0 & \sigma_m \end{bmatrix} \quad (1)$$

Equations in (1) show that the hydrostatic stresses σ_H are driven only by the mean stress σ_m or the pressure p . MAT 24 assumes that hydrostatic stresses cannot generate plastic strains. That is the reason why MAT 24 plasticity model is considered as pressure-insensitive, because the mean stress (or the pressure) cannot induce plastic deformation by definition of the von Mises plasticity model.

The total stress can be always decomposed as the sum of the hydrostatic and deviatoric stresses.

$$\sigma = \mathbf{S} + \sigma_H \quad (2)$$

MAT 24 plasticity model imposes that only the deviatoric stresses \mathbf{S} can develop plastic strains in the material. It turns out that the deviatoric stresses \mathbf{S} are driven only by the equivalent von Mises stress σ_{vm} (i.e. $\|\mathbf{S}\| = \sqrt{\mathbf{S}:\mathbf{S}} = \sqrt{2J_2} = \sqrt{2/3} \sigma_{vm}$. Please refer to [2]).

As a summary, it can be concluded that:

- the hydrostatic stresses σ_H are quantified by the mean stress σ_m
- the deviatoric stresses \mathbf{S} are quantified by the von Mises stress σ_{vm}
- thus, the total stress σ can be quantified with σ_m and σ_{vm}

The σ_{vm} - p diagram helps in the understanding of the material plastic behaviour because it allows to plot the yield stress for each loading mode by means of the scalar physical variables σ_{vm} and p . For MAT 24 and SAMP-1 the σ_{vm} - p diagram represents the yield stress surface.

The loading mode stress triaxiality definition is then naturally defined as:

$$\eta = \frac{\sigma_m}{\sigma_{vm}} = -\frac{p}{\sigma_{vm}} \quad (3)$$

A specific loading mode can be easily represented inside the σ_{vm} - p diagram following the stress triaxiality definition (please refer to equation (4) below).

$$\sigma_{vm} = -\frac{1}{\eta} p \quad (4)$$

Different loading modes can be represented in the σ_{vm} - p diagram as lines which slope will be defined by the inverse of the corresponding loading mode stress triaxiality (affected by the minus sign).

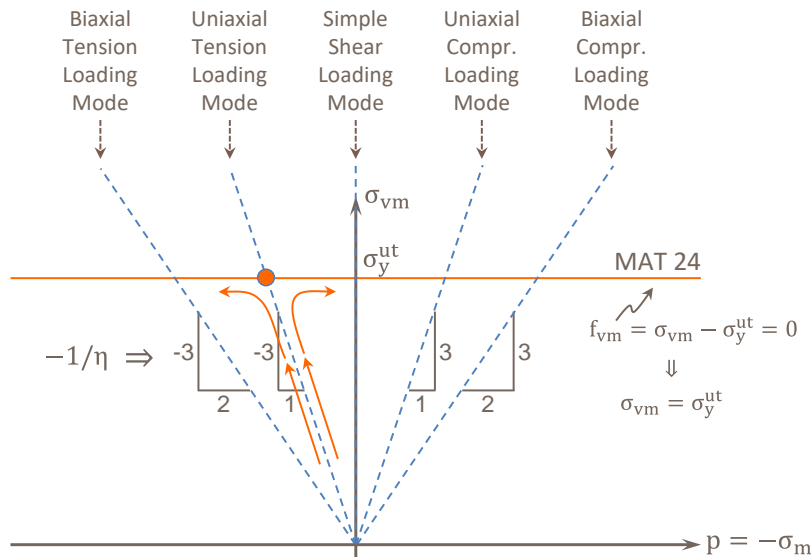
For the particular case of MAT 24 (von Mises plasticity model), the material yields when σ_{vm} equals the uniaxial tension yield stress σ_y^{ut} for all loading modes. This implies that MAT 24 yield surface f_{vm} can be written as:

$$f_{vm} = \sigma_{vm} - \sigma_y^{ut} \quad (5)$$

and the von Mises yield condition is satisfied when $f_{vm} = 0$,

$$\text{Plastic loading} \Rightarrow f_{vm} = 0 \Rightarrow \sigma_{vm} = \sigma_y^{ut} \quad (6)$$

Thus, the MAT 24 yield surface is represented in the σ_{vm} - p diagram as a horizontal line (i.e. no pressure dependency) intercepting the uniaxial tension loading mode line when σ_{vm} equals σ_y^{ut} . The representation of MAT 24 yield surface (i.e. equation (6)) in the σ_{vm} - p diagram is shown in the figure below.



From the σ_{vm} - p diagram above, it is clear why in MAT 24 it is only necessary to define the stress versus plastic strain for the uniaxial tension case to cover the plasticity for all loading modes as a function of the uniaxial tension yield stress evolution.

Regarding MAT 24 yield condition:

- It only depends on the von Mises stress;
- It doesn't depend on the mean stress or pressure;
- It is only driven by the uniaxial tension yield stress which is the single input required;
- The yield stress for the rest of loading modes is imposed by the uniaxial tension one;
- MAT 24 could be classified as a *Single-Loading-mode-Yielding* plasticity model

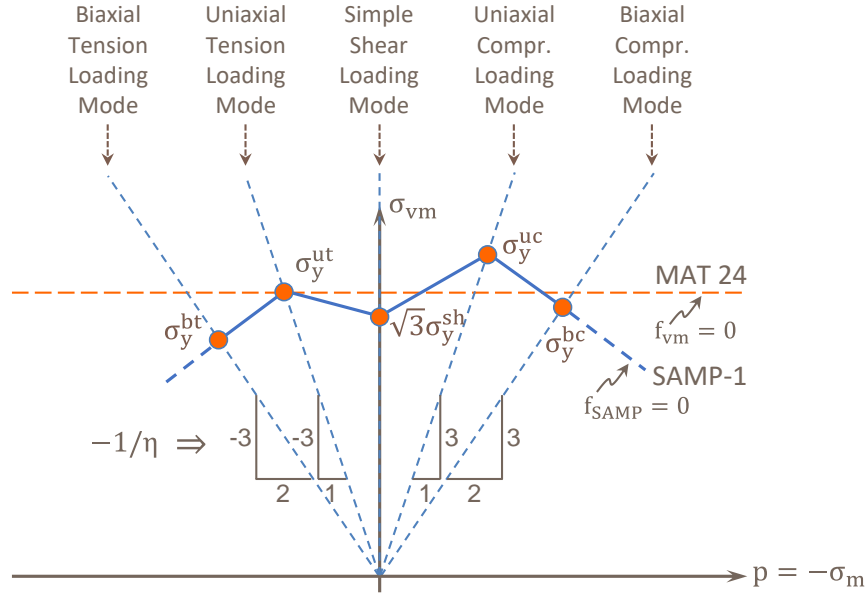
When the material yield stress for different loading modes do not follow MAT 24 plasticity assumptions the following equivalent remarks can be said:

- the material yielding is both shear (i.e. σ_{vm}) and pressure (i.e. p) sensitive
- the material yielding exhibits multi-loading mode dependency
- the material requires a plasticity model that allows the user the definition of independent yield stresses for each loading mode
- The material requires the calibration of a *Multi-Loading-mode-Yielding* material law adjusted to the independent yield stresses of the different loading modes

When the metals plastic behaviour requires a *Multi-Loading-mode-Yielding* material law the use of SAMP-1 is a good solution. The blue yield stress surface in the figure below illustrates a metal with pressure-sensitive plasticity calibrated with SAMP-1 using the piecewise-linear yield surface option with nonzero RBCFAC and four user-input curves LCID-T, LCID-C, LCID-S, and LCID-B defined. In this figure the yield stress surface is driven by the biaxial tension,

uniaxial tension, shear, uniaxial compression and biaxial compression independent yield stresses provided by the user: σ_y^{bt} , σ_y^{ut} , σ_y^{sh} , σ_y^{uc} and σ_y^{bc} respectively.

The σ_{vm} - p diagram below shows a material that exhibits a *Multi-Loading-mode-Yielding* behaviour cannot be modeled with MAT 24 (dashed orange line).



Representing the material yield surface in the σ_{vm} - p diagram provides a simple engineering tool to assess whether MAT 24 is the best fit for the material characterization.

It would be perfect if the coupon test data could be directly represented in the σ_{vm} - p diagram. The main difficulty is that the experimental tests do not provide constant stress triaxiality results and the experimental stress triaxiality cannot be directly measured. Nevertheless, the σ_{vm} - p diagram can be created during the material card generation process to guide the progress of the coupon test matrix correlation.

The simple comparison of the coupon test and component test simulations using MAT 24 versus the experimental results provides a practical tool to find out when the material requires a *Multi-Loading-mode-Yielding* material law. MAT 24 and SAMP-1 results versus the experimental results is included in the following sections.

2.2 Multi-Loading-mode-Yielding definition: Generalized Strength Differential

The *Multi-Loading-mode-Yielding* definition may seem initially complex to define because it involves the definition of the material plastic behaviour for up to 5 loading modes (biaxial tension, uniaxial tension, shear, uniaxial compression and biaxial compression). Nevertheless, using the Strength Differential (SD hereafter) concept the complexity is substantially reduced.

The Strength Differential can be defined as the ratio of the yield stress of a loading mode with respect to the uniaxial tension yield stress. Thus, the SD for the different loading modes read:

• Biaxial tension	$SD_{bt} = \sigma_y^{bt} / \sigma_y^{ut}$	(7)
• Uniaxial tension	$SD_{ut} = \sigma_y^{ut} / \sigma_y^{ut} = 1$	
• Shear	$SD_{sh} = \sigma_y^{sh} / \sigma_y^{ut}$	

- The use of material laws like SAMP-1 is required to accurately capture both
 - the material yield stress evolution for different loading modes and
 - the material plastic strain evolution for different loading modes
- The correlation of the yield stress and plastic strain evolution for different loading modes is the necessary base to properly predict the loading-mode-dependent material fracture behaviour in crashworthiness CAE analysis

Regarding the use of the experimental results in the material card generation:

- Coupon tests do not provide pure loading mode experimental results
- The classic post-process of the experimental stress-strain curves cannot be directly used as SAMP-1 input curves
- Uniaxial tensile test until necking onset is the only input that can be considered as a pure stress state; hence it is the only one that can be partially used as a direct input of SAMP-1 (together with the plastic Poisson's ratio till the necking onset)
- SAMP-1 stress-strain input curves for all pure loading modes need to be obtained by reverse engineering based on the correlation of the coupon experimental results. Reverse engineering is even necessary for the uniaxial tension case after the necking onset for both the stress-strain and the plastic Poisson's ratio evolution

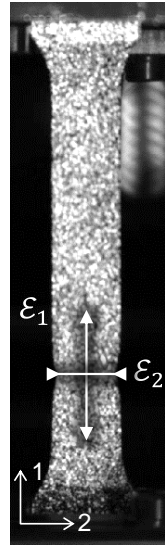
The general uniaxial tension true stress expression valid for small and finite strains without the "constant volume" assumption (assuming $e_{thickness}^{ut} \approx e_2^{ut}$) reads:

$$\sigma_{ut} = \frac{F_{ut}}{A_0(1 + e_2^{ut})^2} = \sigma_{ut}^{eng}(1 + e_1)^{-2} \varepsilon_2 / \varepsilon_1 = \sigma_{ut}^{eng}(1 + e_1)^{2\nu_t} \quad (8)$$

with the total Poisson's ratio ν_t defined as:

$$\nu_t = -\frac{\varepsilon_2}{\varepsilon_1} \quad (9)$$

Being ε_1 and ε_2 the uniaxial tension longitudinal and transverse total true strains. Please note that all the physical variables involved in both the true stress and the total plastic Poisson's ratio can be directly measured from the uniaxial tension test. It is important to remark that these measurements need to be done over a consistent volume to be able to calculate the total Poisson's ratio. For more details, please refer to [1].



The uniaxial tension true stress expression above (i.e. equation (8)) clearly shows that the correct material plastic behaviour calibration in the uniaxial tension case requires the CAE correlation of both:

- the experimental engineering stress σ_{ut}^{eng}
- and the experimental total Poisson's ratio ν_t

The proposed material plastic behaviour calibration for different loading modes can be summarized as follows:

1. For the pure uniaxial tension case:
 - a. generation of the true stress versus the longitudinal plastic strain and
 - b. generation of the plastic Poisson's ratio versus the longitudinal plastic strain

by means of the correlation of both the experimental engineering stress σ_{ut}^{eng} and the experimental total Poisson's ratio ν_t both with respect to the longitudinal plastic strain evolution.

2. Generation of true stress versus plastic strain for:

- pure biaxial tension
- pure shear
- pure compression and
- pure biaxial compression

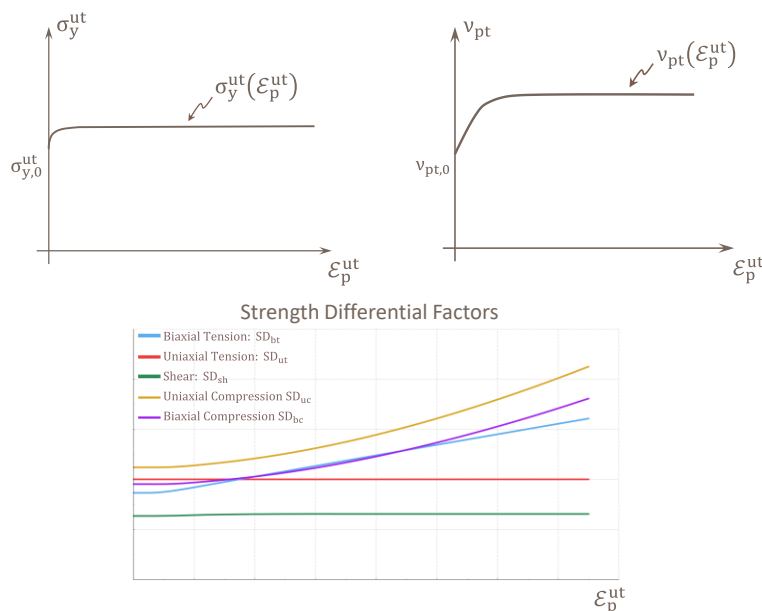
by means of the correlation of the different coupon test experimental results with the calibration of the strength differential factors f_{bt} , f_{sh} , f_{uc} and f_{bc}

This approach allows the CAE engineers the definition of the material yielding behaviour for different loading modes as a group of stress scale factors of the uniaxial tension case. The plastic strain evolution for different loading modes is directly obtained as a function of the uniaxial tension user inputs following the imposed SAMP-1 hardening rule interrelationships. This way, the input consistency is secured.

Once the uniaxial tension test is well correlated, the objective is to obtain the SD factors f_{bt} , f_{sh} , f_{uc} and f_{bc} that maximize the overall coupon test matrix correlation when combined with the Gissmo failure definition. The SD factors don't need to be constant and can vary with the evolution of the uniaxial tension plastic strain.

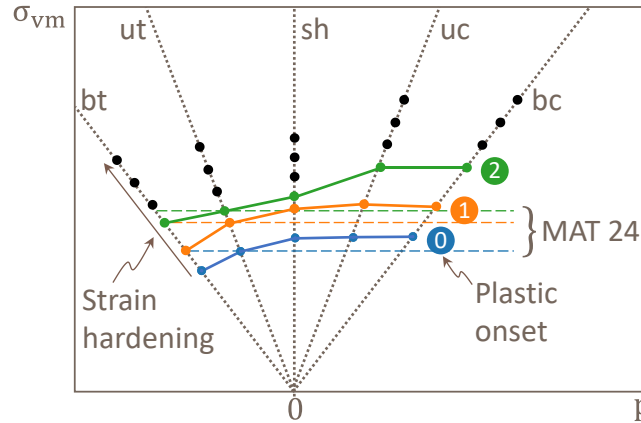
After finalizing the material calibration the user inputs are:

- Stress versus plastic strain for the uniaxial tension case
- Plastic Poisson's ratio versus the uniaxial tension plastic strain
- Strength differential factors for biaxial tension, shear, uniaxial compression, and biaxial compression versus the uniaxial tension plastic strain



The three plots above are the only required user inputs to fully define SAMP-1 material card.

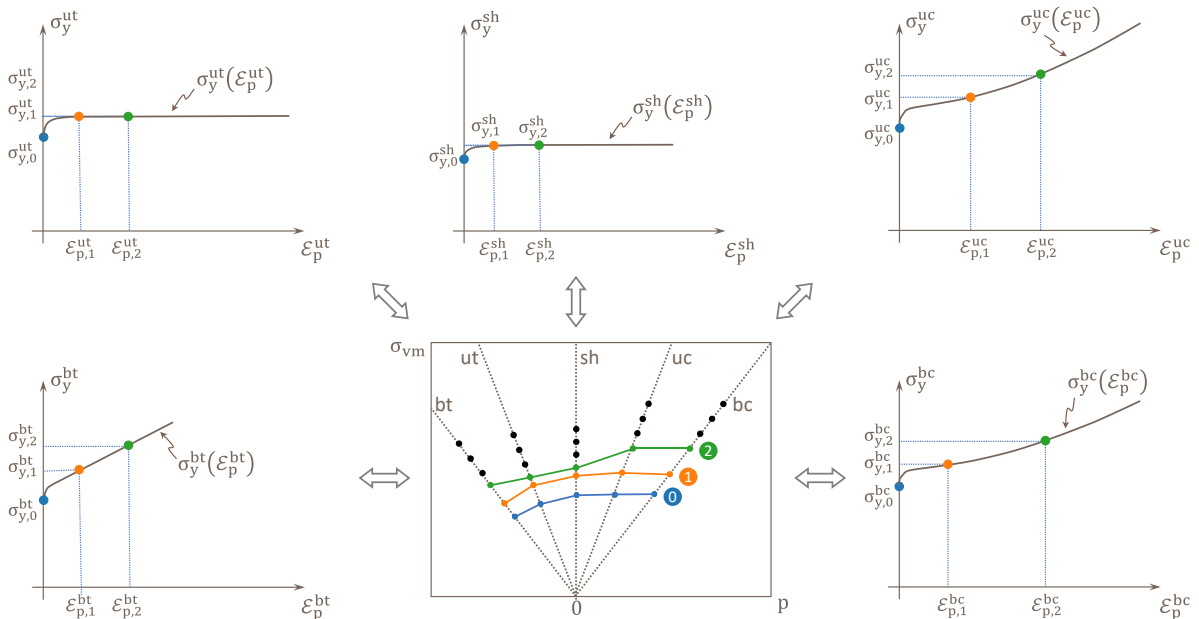
Using the uniaxial tension stress versus plastic strain, the plastic Poisson's ratio, and the different SD factors the material yield stress surface and its strain hardening growth can be directly constructed in the σ_{vm} - p diagram as represented in the figure below.



The SAMP-1 yield stress surfaces represented in the σ_{vm} - p diagram above (i.e. blue, orange, and green solid lines) show that the material doesn't follow MAT 24 plasticity assumptions (i.e. blue, orange, and green dashed lines) neither on the plastic onset nor during the strain hardening yield stress surface growth from ① to ②.

The clear advantage of this approach is that the stress versus plastic strain curves constructed from the different SD factors follow SAMP-1 constitutive model and the numerical consistency of the user inputs is secured.

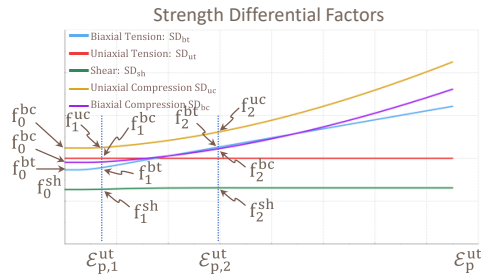
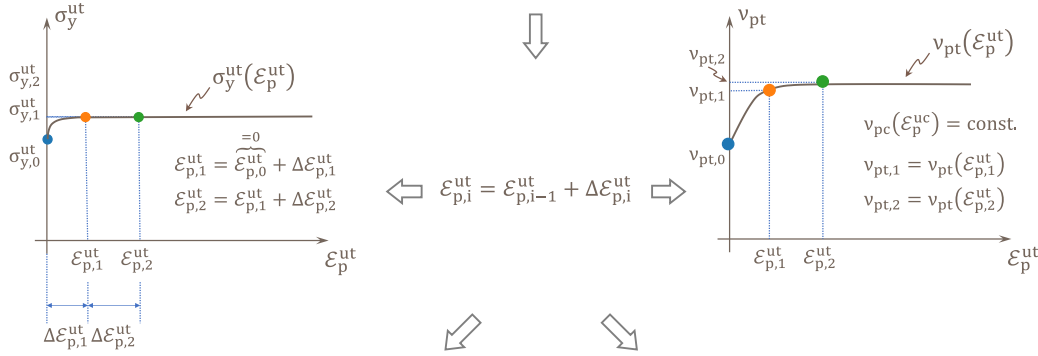
The direct connection between the SAMP-1 stress-strain inputs and its yield stress surface is graphically represented in the figure below. Blue, orange, and green points in the stress-strain curves of different loading modes build up blue, orange, and green yield stress surfaces of the σ_{vm} - p diagram.



The three user inputs (i.e. uniaxial tension stress versus plastic strain, plastic Poisson's ratio and SD factors) is the only information necessary to construct the stress versus plastic strain curves for the rest of loading modes. Plastic compaction considers constant plastic Poisson's ratio ν_{pc} . The construction process of the SAMP-1 stress versus plastic strain input curves for each pure loading mode is graphically shown below. The blue, orange, and green points in the stress-strain plots in the figures above and below belong to the blue, orange, and green yield stress surfaces ①, ② and ③ of the σ_{vm} - p diagram above. The process is illustrated with these points to show a clearer graphic representation, but it is defined to be applied between two consecutive points of the input curves.

$$\varepsilon_{p,i=0}^X = \varepsilon_{p,0}^{ut} = 0 \quad \& \quad \sigma_{y,i=0}^X = f_0^X \sigma_{y,0}^{ut} \quad \text{with } X = \text{bt, sh, uc, bc}$$

For each given $\Delta \varepsilon_{p,i}^{ut}$ while $\varepsilon_{p,i}^{ut} < \varepsilon_{p,\max}^{ut}$

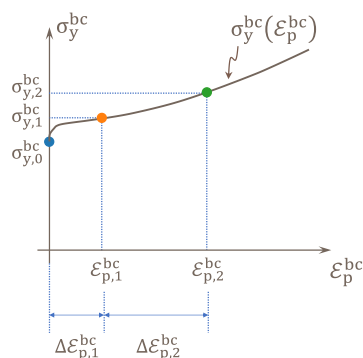
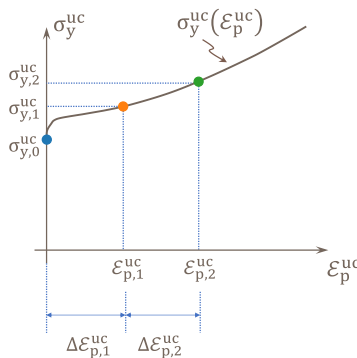
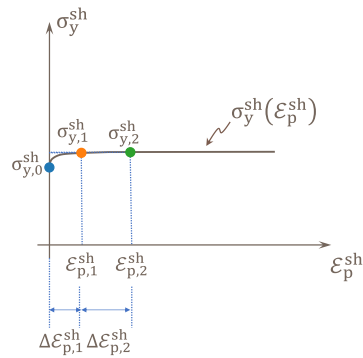
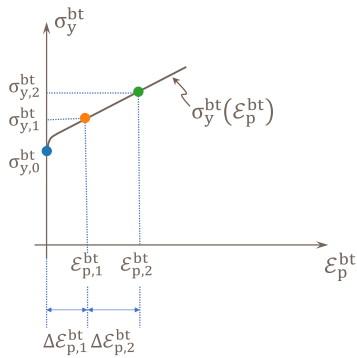


$$\Delta \lambda_i = \frac{\Delta \varepsilon_{p,i}^{ut}}{\sqrt{\frac{3}{2(1+v_{pt,i})}}}$$

$$\Delta \varepsilon_{p,i}^{bt} = \frac{\sqrt{3}}{2} \sqrt{\frac{1-v_{pt,i}}{1+v_{pt,i}}} \Delta \lambda_i \quad \Delta \varepsilon_{p,i}^{uc} = \sqrt{\frac{3}{2(1+v_{pc})}} \Delta \lambda_i$$

$$\Delta \varepsilon_{p,i}^{sh} = \frac{\sqrt{3}}{2} \Delta \lambda_i \quad \Delta \varepsilon_{p,i}^{bc} = \frac{\sqrt{3}}{2} \sqrt{\frac{1-v_{pc}}{1+v_{pc}}} \Delta \lambda_i$$

$$\begin{aligned} \sigma_{y,i}^{bt} &= f_i^{bt} \sigma_{y,i}^{ut} & \varepsilon_{p,i}^{bt} &= \varepsilon_{p,i-1}^{bt} + \Delta \varepsilon_{p,i}^{bt} \\ \sigma_{y,i}^{sh} &= f_i^{sh} \sigma_{y,i}^{ut} & \varepsilon_{p,i}^{sh} &= \varepsilon_{p,i-1}^{sh} + \Delta \varepsilon_{p,i}^{sh} \\ \sigma_{y,i}^{uc} &= f_i^{uc} \sigma_{y,i}^{ut} & \varepsilon_{p,i}^{uc} &= \varepsilon_{p,i-1}^{uc} + \Delta \varepsilon_{p,i}^{uc} \\ \sigma_{y,i}^{bc} &= f_i^{bc} \sigma_{y,i}^{ut} & \varepsilon_{p,i}^{bc} &= \varepsilon_{p,i-1}^{bc} + \Delta \varepsilon_{p,i}^{bc} \end{aligned}$$

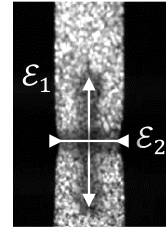


The overall approach described above could be also understood as a generalized SAMP-Light where the user defines the different SD factors for each loading mode.

4 CAE correlation at coupon & component level

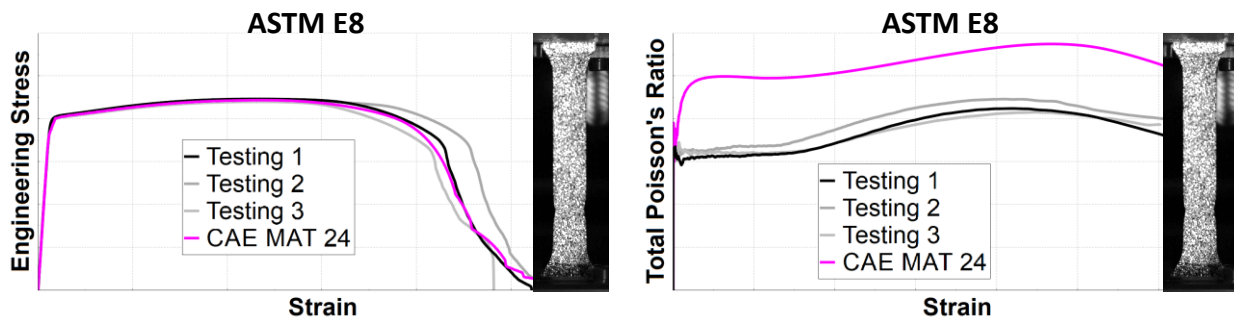
4.1 MAT 24 plus GISSMO: Single-Loading-mode-Yielding

As it is explained in previous sections of this paper, the uniaxial tension true stress expression (i.e. equation (8)) shows that the correct material plastic behaviour calibration for the ASTM E8 coupon test requires the CAE correlation of the evolution of the experimental engineering stress and the experimental total Poisson's ratio $\nu_t = \varepsilon_2/\varepsilon_1$ both versus the longitudinal strain ε_1 .



The total Poisson's ratio in the plastic region cannot be controlled by the user in MAT 24 because MAT 24 assumes and imposes constant volume plasticity (i.e. constant $\nu_p = 0.5$). Thus, the total Poisson's ratio measured in the CAE coupon test is just an output of the simulation when using MAT 24.

A MAT 24 plus Gissmo is calibrated for plastic and fracture behaviour to correlate the uniaxial tension coupon tests of the aluminium alloy studied in this paper. The figures below show MAT 24 plus Gissmo correlation for the uniaxial tension ASTM E8 coupon test.

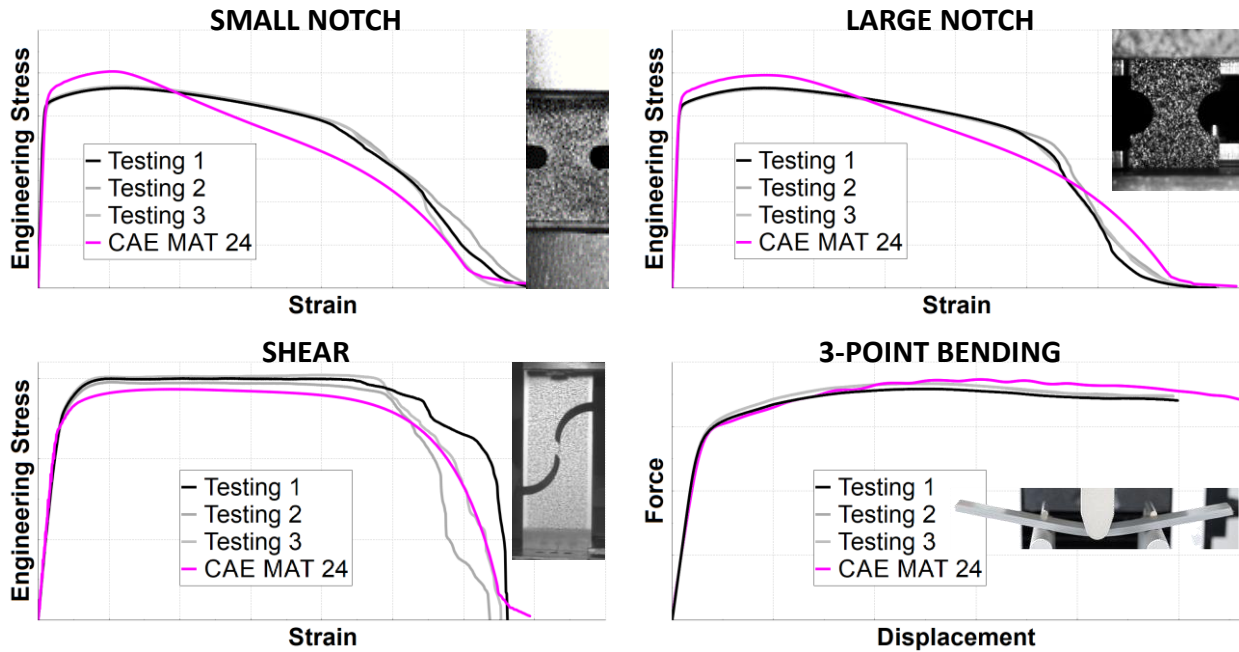


ASTM E8 coupon test. CAE correlation for MAT 24. Courtesy of Faraday Future

The CAE results above show that MAT 24 is a good tool for capturing the engineering stress versus the longitudinal strain but the total Poisson's ratio evolution exhibits a poor correlation level. Thus, the complete correlation of the ASTM E8 coupon tests cannot be achieved with MAT 24.

The lack of correlation of the experimental total Poisson's ratio also highlights that the studied aluminium alloy does not exhibit constant volume plasticity. Thus, a material card like SAMP-1 is necessary to properly capture the necking behaviour.

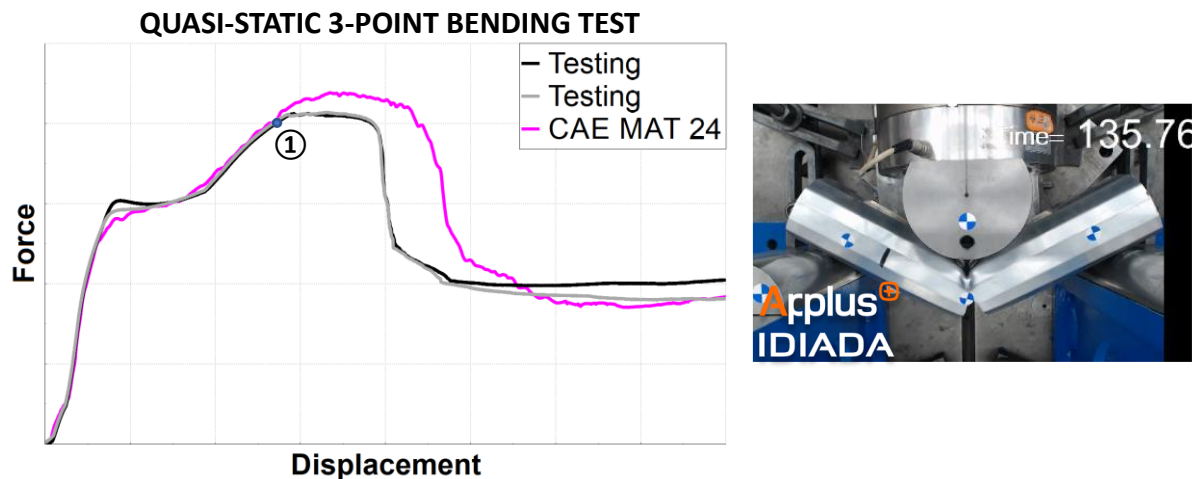
In MAT 24 the user can only define the stress versus plastic strain for the pure uniaxial tension case. Thus, the plastic behaviour for the rest of loading modes is again just an output of the simulation. The figures below show the correlation level of the same MAT 24 for the rest of coupon tests.



Coupon test matrix. CAE correlation for MAT 24. Courtesy of Faraday Future

The level of correlation of MAT 24 for the rest of coupon tests confirms that MAT 24 is not able to predict a Multi-Loading-mode-Yielding material behaviour. Large Notch and Small Notch are the coupon tests where MAT 24 exhibits worse predictivity since the yield stress onset and the stress evolution before necking are severely overestimated, and the post necking behaviour is clearly penalized by the lack of correlation of the total Poisson's ratio. Low correlation is also exhibited in the shear tests. In the 3-point bending tests the plastic behaviour is driven by the plastic tension loading and the correlation level is acceptable.

The figure below shows the correlation of the 3-point bending component test using the same MAT 24 (component test setup described in the following section 4.2).



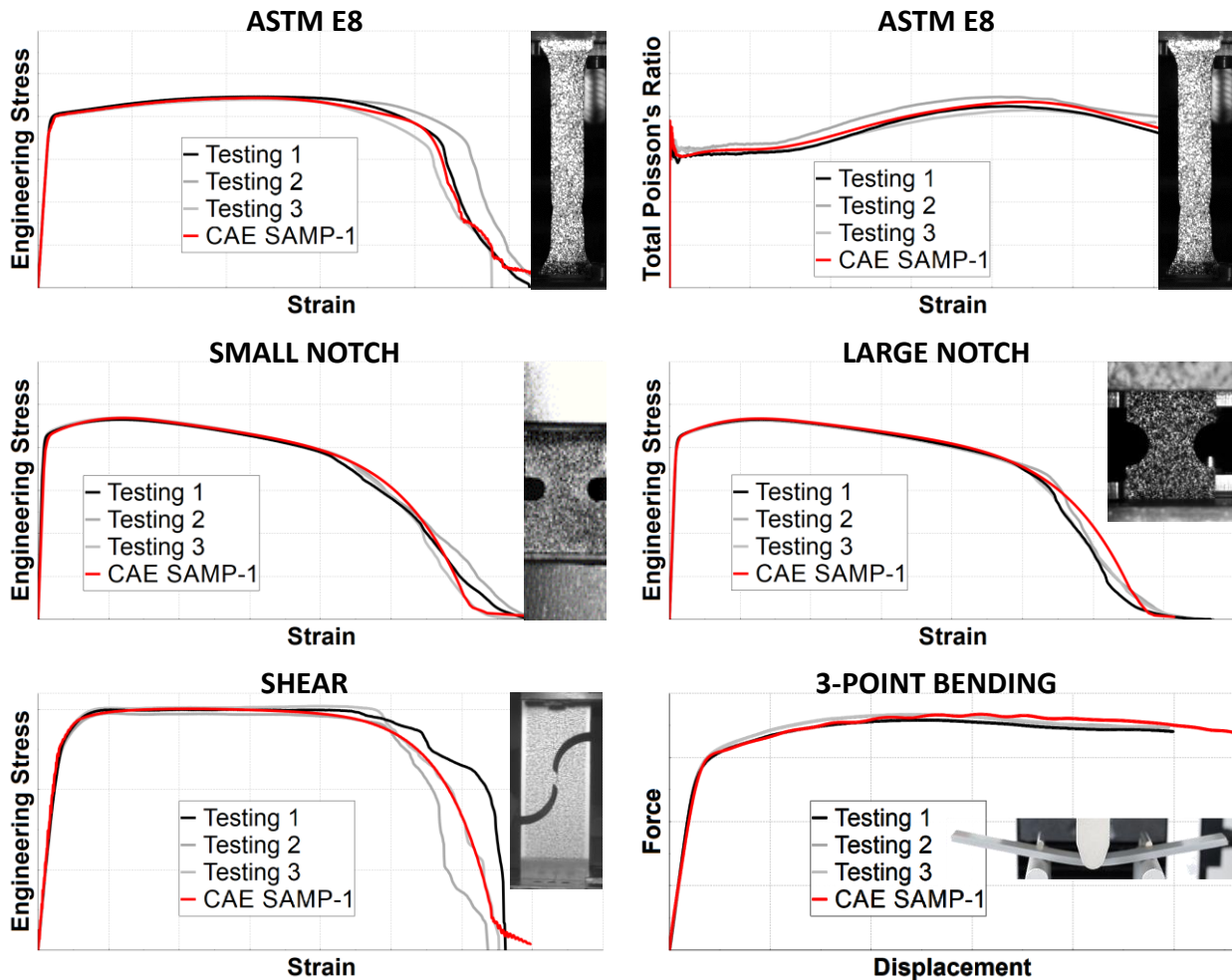
CAE correlation quasi-static 3-point bending tests using MAT 24. Courtesy of Faraday Future

The correlation level is acceptable in the first part of the force-displacement curve but there is a significant deviation from the experimental results when the component is close to the fracture onset (from point ① in the plot onwards). These results confirm that the calibration of the material plasticity for different loading modes is the necessary base to properly predict the

loading-mode-dependent material fracture at component level in crashworthiness CAE analysis.

4.2 SAMP-1 plus GISSMO: Multi-Loading-mode-Yielding

The CAE correlation at coupon level using SAMP-1 plus GISSMO is shown in the figures below.



Coupon test matrix CAE correlation for SAMP-1. Courtesy of Faraday Future

The CAE versus Testing correlation above shows that the *Multi-Loading-mode-Yielding* approach based on SD factors in combination with the proper Gissmo calibration provides a robust engineering tool to capture the material crash behaviour at coupon level.

The component level activities are required for the definition of the component CAE modeling guidelines for both bending and axial crush driven crash load cases. Additionally, the component level activities validate the coupon level material card.

The figures below show the component test setups for the quasi-static 3-point bending tests and the axial crush impact test both carried out at IDIADA's Labs.



Component test setup for quasi-static 3-point bending tests. Courtesy of Faraday Future

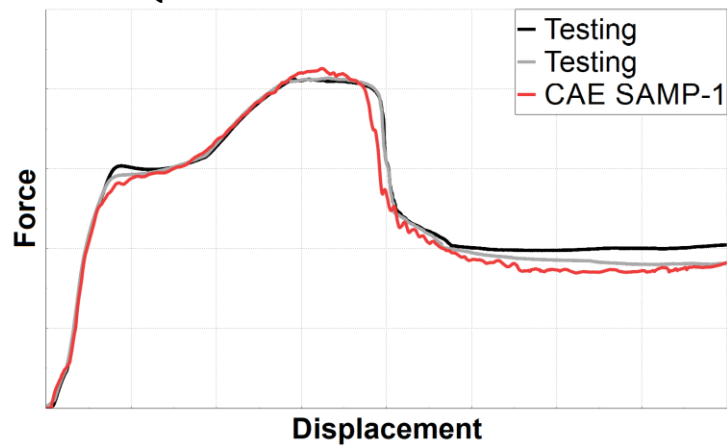


Component test setup for axial crush impact tests. Courtesy of Faraday Future

The axial crush impact tests were carried out at IDIADA's crash laboratory setting up a guided impact system with a total mass of 1100 kg and an impact velocity of 48 km/h.

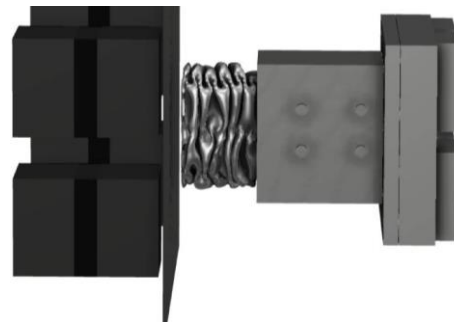
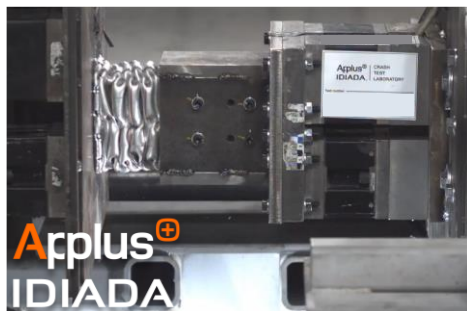
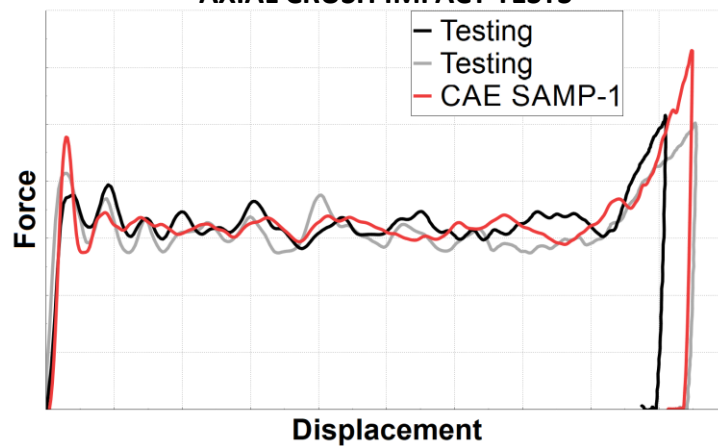
The correlation results at component level are presented in the figures below.

QUASI-STATIC 3-POINT BENDING TEST



CAE correlation quasi-static 3-point bending tests using SAMP-1. Courtesy of Faraday Future

AXIAL CRUSH IMPACT TESTS



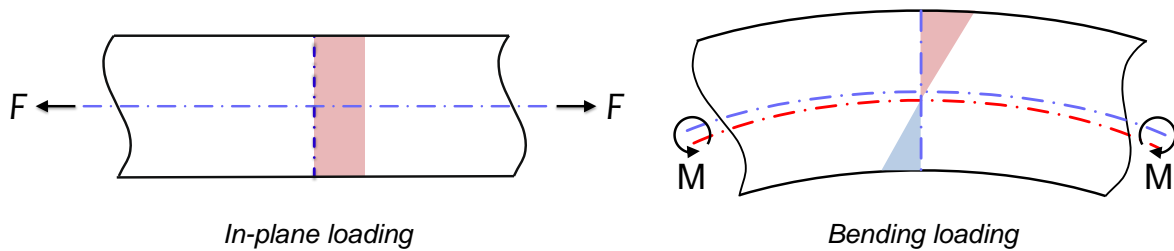
CAE correlation axial crush impact test using SAMP-1. Courtesy of Faraday Future

The CAE versus Testing correlation at component level validates the engineering approach.

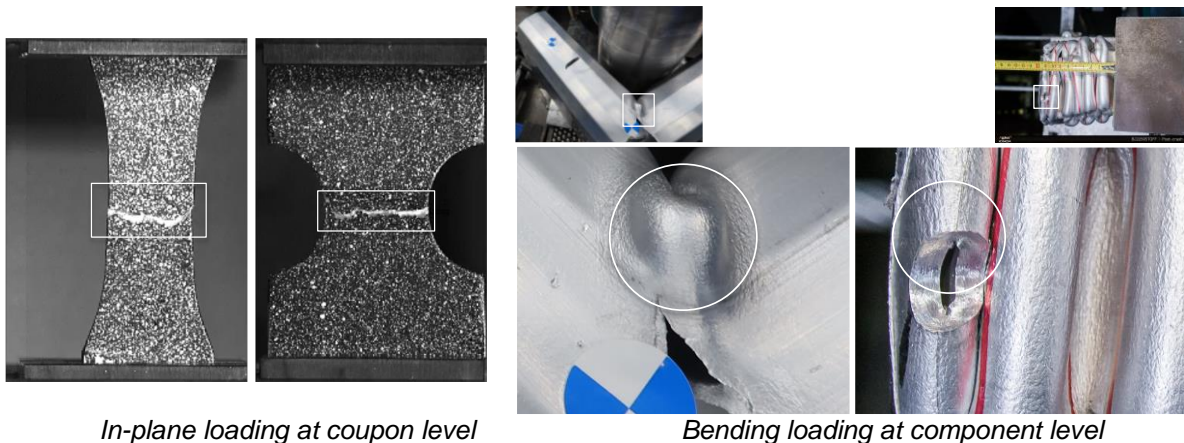
5 In-plane loading versus bending loading in metal deformation and failure

One of the main objectives in metals characterization for crash CAE analysis regarding the prediction of the material deformation and failure is that the CAE material cards used for car body components maintain the accuracy achieved in the calibration at coupon level.

In full vehicle crash impacts the car body components can work, deform, and potentially fail under in-plane loading and bending loading. In-plane loading is understood as the group of loading conditions that induce tensile yield stress distributions through the thin-wall thickness. Bending loading considers the group of loading conditions that make the thin-wall plastically bend. Bending loading induces a stress gradient through the thickness from yield tension at one of the skin faces to yield compression at the opposite skin face. In-plane and bending loading modes are illustrated in the figures below.



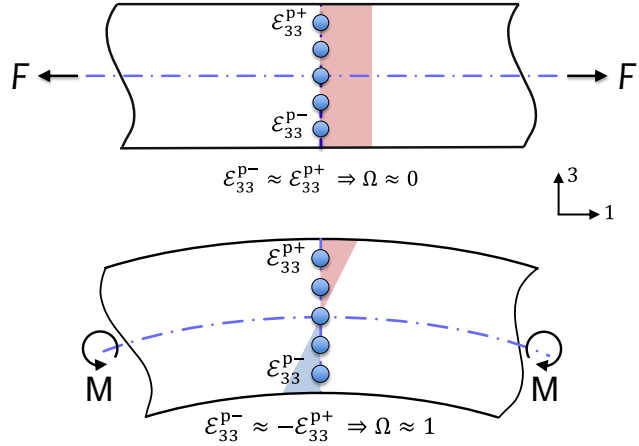
Most of the coupon test setups described in this paper make the material work under in-plane loading. However, plastic deformation and failure under bending loading may drive the car body structural performance in several crash scenarios. The figures below illustrate in-plane loading at coupon level and bending loading at component level for 3-point bending and axial crush conditions.



The levels of plastic deformation before failure in the plastically bent component areas (highlighted with white circles in the right figures above) are several times larger than the failure deformation levels observed in in-plane loading at coupon level (highlighted with white rectangles in the left figures above).

It turns out that bending loading does not induce necking, allowing the material to generate a distributed multi-micro-crack region commonly referred to as “elephant skin”. Elephant skin regions can accommodate a significantly higher levels of plastic deformation before failure than the localized deformations before failure seen in in-plane loading conditions. Thus, metal material cards calibrated exclusively based on in-plane loading from coupon tests may result in early brittle component failure in the plastically bent regions during full vehicle crash CAE analysis.

The implementation of in-plane versus bending loading material behaviour inside the CAE material cards is a key factor to secure that a single material card delivers the same failure prediction accuracy at both coupon and component level. The bending index parameter Ω in Gissmo facilitates the calibration of the material cards differentiating between in-plane and bending loading deformation and failure.

$$\Omega = \frac{1}{2} \frac{|\varepsilon_{33}^{p+} - \varepsilon_{33}^{p-}|}{\max(|\varepsilon_{33}^{p+}|, |\varepsilon_{33}^{p-}|)}$$


Bending Index Ω

6 Conclusions

The engineering process described in this paper demonstrates that advanced plasticity approaches can be effectively used with minimal impact on the complexity of material characterization. The coupon test matrix performed for GISSMO fracture model can be used for SAMP-1 Multi-Loading-mode-Yielding plasticity calibration.

The proposed Testing and CAE methods for plastic and fracture characterization are focused on crash performance and highlights the importance of assessing the material yielding dependence on different loading modes and evaluates the suitability of MAT 24 and SAMP-1.

The method based on the Strength Differential concept offers a simplified and user-oriented approach that secures user-inputs consistency and enhances accuracy of material characterization in crashworthiness CAE analysis for car body structural metals. The methodology is experimentally validated at coupon and component level for shell-based crash CAE models.

The overall process explained in this paper illustrates IDIADA's approach of tailor-defined Testing and CAE methods for crash performance validation at coupon, component, subsystem, and full vehicle level applying a Dynamic Building Block Approach. The Dynamic Building Block Approach vertically integrates virtual and physical development tools for providing complete product engineering solutions.

7 Acknowledgements

IDIADA would like to extend its sincere thanks to Faraday Future for permitting the presentation of the coupon and component experimental data in this paper. Their contribution has been invaluable to the success of this project. We want to thank Andrew Hall, Patrick Kelly, Ilyasuddin Syed, Jose Luis Cardini and Irmantas Burba for their support throughout the entire project.

8 Correspondence

Alejandro Domínguez
Lead Engineer, Materials Engineering
E-mail: Alejandro.Dominguez@idiada.com

Pablo Cruz
Senior Manager Body & Passive Safety
E-mail: Pablo.Cruz@idiada.com

9 Literature

- [1] Steven M. Arnold, Bradley Lerch and Trenton M. Ricks 2019: Interpretation of Experimental Tensile Test Results and Its Implication on Damage Modeling.
- [2] H. Altenbach, A. Öchsner. (2014). Plasticity of Pressure-Sensitive Materials. 10.1007/978-3-642-40945-5.
- [3] P. Cruz et al. 2021. Non-Isochoric Plasticity Assessment for Accurate Crashworthiness CAE Analysis. Application to SAMP-1 and SAMP-Light. 13th European LS-DYNA Conference 2021 (https://www.dynalook.com/conferences/13th-european-ls-dyna-conference-2021/material-modeling/cruz_applus_idiada.pdf).
- [4] RI Borja 2013: Plasticity. Modeling & Computation
- [5] EA de Souza Neto et al. 2008: Computational Methods For Plasticity. Theory And Applications.
- [6] S. Kolling, A. Haufe, M. Feucht, P. Du Bois. (2005). SAMP-1: A Semi-Analytical Model for the Simulation of Polymers.
- [7] M. Vogler, S. Kolling, A. Haufe. (2007). A Constitutive Model for Plastics with Piecewise Linear Yield Surface and Damage.
- [8] José E. Andrade. Plasticity at Caltech.
- [9] M. Benz, J. Irslinger, M. Feucht, P. Du Bois, M. Bischoff. (2019). Development of a New Method for Strain Field Optimized Material Characterization.
- [10] J. Lubliner. (2006). Plasticity Theory.
- [11] J.C. Simo, T.J.R. Hughes. (1998). Computational Inelasticity.
- [12] Drucker, D.C. (1973). Plasticity theory strength-differential (SD) phenomenon, and volume expansion in metals and plastics. Metall Mater Trans B 4, 667.
- [13] Jens Kristian Holmen, Bjørn Håkon Frodal, Odd Sture Hopperstad, Tore Børvik. (2017). Strength differential effect in age hardened aluminum alloys. International Journal of Plasticity, Volume 99, Pages 144-161, ISSN 0749-6419. <https://doi.org/10.1016/j.ijplas.2017.09.004>.